Journal of Advanced Ceramics
先进陶瓷
ISSN 2226-4108
CN 10-1154/TQ
清華大学出版社 Tsinghua University Press
SciOpen

J Adv Ceram 2026, **15**: 9221411

https://doi.org/10.26599/JAC.2026.9221411

Rapid Communication

Achieving room temperature plasticity in TiO_2 ceramics by flash processing

Xinghua Su [1,*], Zhenyu Li [1], Xufei Fang [2], Wenjun Lu [3], Mengyao Wang [1], Peng Zhao [1]

[1] *School of Materials Science and Engineering, Chang'an University, Xi'an 710061, China*

[2] *Institute for Applied Materials, Karlsruhe Institute of Technology, Karlsruhe 76131, Germany*

[3] *Department of Mechanical and Energy Engineering, Southern University of Science and Technology, Shenzhen 518055, China*

* Corresponding author.

E-mail: suxinghua@chd.edu.cn

Received: October 8, 2026; Revised: November 1, 2026; Accepted: November 18, 2026

©The Author(s) 2026

Just Accepted

Abstract:

Ceramics are indispensable materials for modern engineering and high-technology applications. However, the intrinsic brittleness at room temperature can cause catastrophic failure and severely limit their widespread applications. Here, we report a flash processing (FP) method based on the coupling of electric and thermal fields to significantly improve the room-temperature plasticity of TiO_2 ceramics with a large plastic compressive strain of 15.4% during micropillar compression. This large room-temperature plasticity is attributed to the proliferation of stacking faults and twin boundaries during the loading process, which may be assisted by the high concentration of oxygen vacancies introduced by the FP method. Our findings suggest that FP can be a simple and effective method for achieving improved room-temperature plasticity of ceramic materials through defect engineering.

Keywords: room-temperature plasticity; flash processing; TiO_2; micropillar compression; stacking faults

Just Accepted

1 Introduction

Advanced ceramics are indispensable materials for modern engineering and high-technology applications, owing to their superior mechanical strength, chemical stability, and high-temperature capability [1-5]. However, the widespread structural application of ceramics is fundamentally bottlenecked by their inherent catastrophic brittleness at room temperature. Unlike metals, the strong ionic and covalent bonds in

ceramics often impose a very high Peierls-Nabarro stress, which severely hinders dislocation mobility at room temperature, even if dislocation nucleation can be circumvented [6,7]. Consequently, under external mechanical loading, stress concentration at the pre-existing flaws, dislocation pileups, or crack tips inevitably triggers premature, catastrophic failure before occurrence of appreciable plastic deformation. Overcoming this intrinsic brittleness and achieving room-temperature plasticity has remained a long-standing challenge.

Over the past decades, intensive efforts have been dedicated to mitigating ceramic brittleness, primarily through extrinsic toughening mechanisms such as phase transformation [8], grain refinement [9], and the introduction of secondary phases [10]. While these strategies successfully enhance fracture toughness, they rarely alter the intrinsic deformation capability of the ceramic bulk itself. Intrinsic plastic deformation in ceramics typically requires high temperatures (usually above half of their melting points) to thermally activate slip systems, dislocation motion, and grain boundary sliding [11-14]. As a result, defects engineering, which involves introducing abundant defects (particularly dislocations) into ceramics, has been presented to achieve plasticity in ceramics at room temperature [15-17]. For example, Dong et al. achieved the exceptional tensile ductility exceeding 39.9% in La_2O_3 ceramics at room temperature using a concept of “borrowed-dislocations”, which entailed continuously transmitting dislocations from Mo metals and introducing them into La_2O_3 ceramics [15]. Fang et al. reported the room-temperature plasticity up to 32% in $SrTiO_3$ through mechanically seeded dislocations [16]. Shen at al. proposed an elevated temperature

Just Accepted

preloading method to introduce abundant defects into the TiO_2 ceramics, and achieved a 10% compressive strain at room temperature [17]. However, these approaches for introduction of defects require stringent pre-deformation or processing conditions, and are limited to specific material systems. Challenges in scalability remain. Therefore, it is necessary to develop more generalized methods to improve the plasticity of ceramics at room temperature.

Recently, the emergence of a novel field-assisted sintering technique, namely flash sintering, has revolutionized the synthesis and sintering of ceramic materials [18-21]. By applying a critical electric field accompanied by heating, flash sintering enables ultra-fast densification and solid-state reaction within seconds at significantly lowered furnace temperatures. For example, Cologna et al. demonstrated that yttria-stabilized zirconia (YSZ) could be rapidly densified to full density within only a few seconds at 850 °C via flash sintering [18]. More remarkably, Liu et al. reported that ZnO ceramics could be densified by flash sintering even at room temperature [22]. Recently, Su et al. successfully fabricated dense high-entropy rare-earth zirconate ceramics via flash sintering of a mixture of oxide powders at 865 °C for 60 s, during which solid-state reactions and densification proceeded simultaneously [23]. Beyond its unprecedented efficiency in sintering, the coupling of electric and thermal fields has been found to induce extraordinary non-equilibrium states, including massive point defect generation, accelerated diffusion kinetics, and altered grain boundary energy [24-29]. Emerging evidence suggests that these electro-thermal coupled fields can profoundly interact with the defect chemistry and defects kinetics of ceramics.

Just Accepted

However, the exploration of flash technique has been predominantly confined to the densification stage. Whether such a unique electro-thermal coupling can be exploited to fundamentally reshape the mechanical response, specifically to unlock room-temperature plasticity, remains largely unexplored.

In this work, we report an electro-thermal coupled flash processing (FP) strategy to significantly improve the room-temperature plasticity of ceramics, as showcased on TiO_2. Differs from the flash sintering, FP operates directly on already densified ceramics rather than porous green bodies. Moreover, instead of driving densification, the FP is leveraged for microstructural tuning via defect engineering, providing a versatile platform to tune the physical-chemical properties of ceramic materials. Titanium dioxide (TiO_2), a classic transition metal oxide with high industrial relevance, typically exhibits a highly brittle nature under ambient conditions. The brittle to ductile transition temperature of bulk TiO_2 crystals was reported to be higher than 600 °C [30], much higher than room temperature. Here in this work, we show that after FP, TiO_2 demonstrates substantial plastic strain under mechanical loading at room temperature, completely deviating from the conventional brittle fracture behavior.

Detailed structural characterization reveals that the TiO_2 after FP contains a minor fraction of pre-existing stacking faults and twins, alongside a high concentration of oxygen vacancies. During room-temperature compression, the multiplication of these stacking faults and twin boundaries drive the significant room-temperature plasticity. The proliferation of these planar defects is strongly assisted by the abundant oxygen

Just Accepted

vacancies, which likely facilitate their nucleation and growth. Different from the previously reported dislocation-assisted room-temperature plasticity, our findings uncover a novel oxygen-vacancy-assisted stacking fault and twinning proliferation route for improving ceramic plasticity. Our findings not only suggest that FP can be a facile and effective method to improve the room-temperature plasticity of ceramic materials, but also helpful to deeply understand the deformation mechanisms of ceramic materials.

2 Materials and methods

2.1 Flash processing

Rutile TiO_2 bulk samples (relative density of 98.2%) with a diameter of ~6.2 mm and a thickness of ~2.8 mm were used as pristine samples. The samples were first ground with 4000-grit silicon carbide abrasive paper and then polished with a diamond suspension. After that, ultrasonic cleaning was performed for 10 min to remove contaminants. The dense TiO_2 samples were sandwiched between two Cu sheets as electrodes. To ensure rigid contact between the sample and the electrode, a pressure of approximately 50 kPa was applied to the electrodes through the alumina plates and rods. A DC power supply (HPS0614, Hangzhou Lanyi Electronics Co., Ltd., China) was used to apply a constant electric field of 500 V cm^{-1} to the samples. Then the samples were heated in a furnace at a rate of 10 °C min^{-1} in air. When the current flowing through the sample increased rapidly to preset values of 230 and 280 mA (corresponding to a current density of 0.762 and 0.928 A cm^{-2}, respectively), which signaled the occurrence of the flash event. At the same time, the power supply was

Just Accepted

switched from the voltage-control mode to the current-control mode. The sample was then kept at a constant current state for 60 s. After that, the power supply and furnace were turned off, and the samples were furnace cooled to room temperature.

2.2 Micropillar compression test

TiO_2 micropillars with ~3 μm in diameter and ~6 μm in height were prepared from the TiO_2 sample near the anode side using a Thermo Fisher Scios 2 Dual Beam Scanning Electron Microscope-Focused Ion Beam (SEM-FIB). The micropillars were prepared under the following sequence of FIB parameters: rough cutting at 30 kV and 7 nA, fine polishing at 30 kV and 50 pA, and final low-voltage cleaning at 5 kV and 23 pA to minimize surface damage. In situ micropillar compression tests were performed using a nanomechanical testing system (FT-NMT04, FemtoTools) in displacement-controlled mode at a constant strain rate of 1×10^{-4} s^{-1}. The compression tests were continued until sample failure, which was marked by the appearance of visible cracking and sudden load drops. All the measured displacement data were rigorously corrected for system compliance prior to strain calculation.

2.3 Sample characterizations

Microstructure characterization was performed on a transmission electron microscope (TEM, Thermofisher Talos F200X) operated at 200 kV. TEM samples of TiO_2 with FP were prepared through the conventional cutting, grinding and ion milling. Specifically, the TEM foils were first mechanically polished to 30 μm thick, followed by ion milling (Gatan 695) with an incident beam angle of 6° at 4 kV until the hole appeared. Finally, the foils were Ar ion milled with an angle of 3° at 3 kV for

Just Accepted

20 min. For samples post-micropillar compression, cross-section TEM samples were fabricated using a Thermo Fisher Scios 2 Dual Beam SEM-FIB system. The crystalline structure was identified by an X-ray diffractometer (XRD; D8 Davinci, Bruker, Germany) with Cu Kα radiation. Electron paramagnetic resonance (EPR) spectroscopy was carried out to detect oxygen vacancies using an A300 spectrometer (Bruker, Germany). The X-ray photoelectron spectroscopy (XPS) was performed on an ESCALAB 250 spectrometer (Thermo VG Scientific, USA) with monochromatic Al Kα excitation. It should be noted that the XRD, EPR and XPS were carried out on the region near the anode side of the sample.

3 Results

The schematic of flash processing (FP) is illustrated in Fig. 1. Initially, a constant electric field of 500 V cm^{-1} was applied to the dense TiO_2 samples. Subsequently, the TiO_2 samples were heated in air. Upon reaching a temperature of ~575 °C, the electrical conductivity of the sample increased non-linearly, causing the current passing through the sample to surge rapidly to a preset limit (230 and 280 mA, corresponding to a current density of 0.762 and 0.928 A cm^{-2}, respectively). Thereafter, the sample was held under this constant current for 60 s (Fig. 1(b)). It should be noted that, due to the Joule heating effect, the actual temperature of the sample is higher than the furnace temperature during FP. According to the black body radiation model [31], the actual sample temperature in the FP at 230 and 280 mA is estimated to be 749 and 803 °C, respectively. Furthermore, after the FP, the color of the TiO_2 sample became slightly darker, as shown in the inset of Fig. 1(b).

Just Accepted

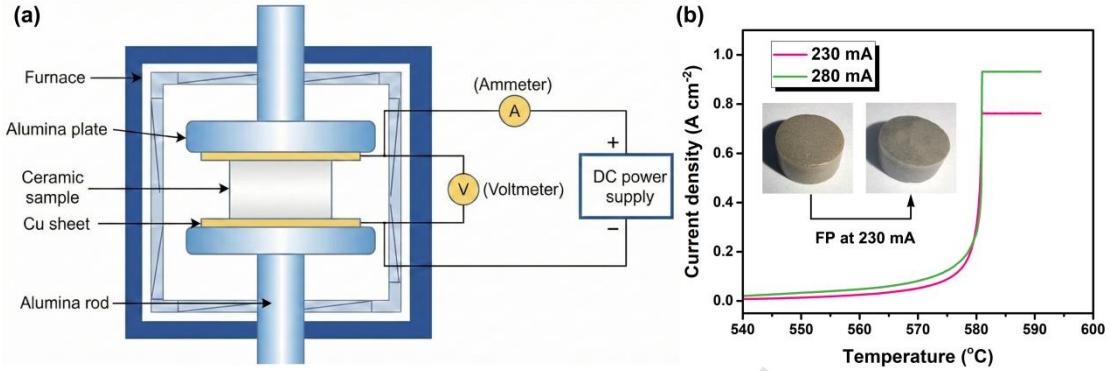


Fig. 1 (a) Schematic experimental setup for FP. (b) Current density as a function of temperature during FP. The inset shows photographs of the TiO_2 samples before and after FP at 230 mA.

Micropillar compression tests of TiO_2 samples without FP and with FP at 230 and 280 mA were performed at room temperature with a constant strain rate of 1×10^{-4} s^{-1}. For the pristine TiO_2 sample without FP, pillars experienced brittle catastrophic failure at an engineering strain of ~2.3% and an engineering stress of 3.6 GPa (Fig. 2(a-d)). The crack expansion was instantaneous and catastrophic (see supplementary Movie S1 for detail). In contrast, pillars underwent plastic deformation for the TiO_2 sample with FP at 230 mA (Fig. 2(e-h)). Serrations are clearly observed on the stress-strain curves, which are due to significant plastic deformation prior to failure. A maximum strain of ~15.4% (red curve in Fig. 2(e)) is achieved without noticeable major cracks. From the in situ SEM snapshots of a representative pillar, it can be seen that shear bands are formed and propagated throughout the entire pillar under successive compression (see supplementary Movie S2 for detail).

Interestingly, for the TiO_2 sample with FP at 280 mA, the stress-strain curves exhibit a pronounced work-hardening behavior (Fig. 2(i-l)), which is rarely observed in ceramic materials during deformation. The flow stress is increased continuously to

Just Accepted

3.5 GPa under loading, and the engineering strain reaches 14.7% without brittle fracture (see supplementary Movie S3 for detail). Similarly, the generation and proliferation of shear bands occur during the compression process (Fig. 2(j-l)).

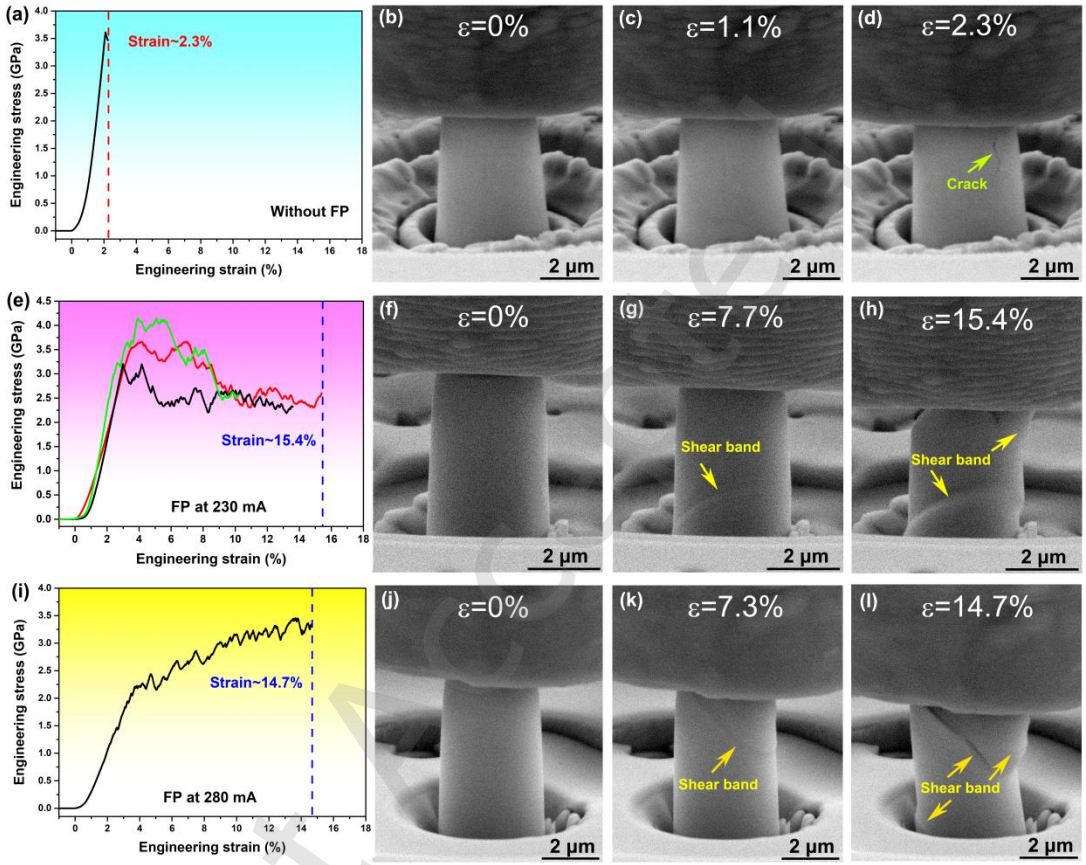


Fig. 2 Uniaxial in situ microcompression tests at room temperature. (a-d) Stress-strain curve of TiO_2 without FP. (e-h) Stress-strain curves of TiO_2 with FP at 230 mA from different individual pillars. (i-l) Stress-strain curve of TiO_2 with FP at 280 mA.

To investigate the microstructural evolution during compressive deformation, TEM characterization was performed on TiO_2 samples (FP at 280 mA) subjected to compressive strains of 8.0% and 14.7%. For the pillar compressed to a strain of 8.0%, several parallel slip bands are observed (Fig. 3(a)). To further examine the microstructure in detail, the region highlighted by the red box in Fig. 3(a) is selected for TEM characterization. It is revealed that these parallel slip bands consist of

stacking faults and twin boundaries, which is confirmed by the spot splitting and streaking lines in the selected-area electron diffraction (SAED) pattern (Fig. 3(b)). High-resolution TEM (HRTEM) image of the region in Fig. 3(b) (indicated by the red box) shows that stacking faults are localized at the twin boundary, which is further confirmed by the inserted fast Fourier transformation (FFT) pattern (Fig. 3(c)).

For the pillar compressed to a strain of 14.7%, a high density of parallel slip bands is observed in the deformed region (Fig. 3(d)). In addition, no cracks are observed. These abundant slip bands intersected with the surface of the pillar and resulted in prominent shear offsets, as shown in Fig. 2(l). In Fig. 3(e), it reveals that these parallel slip bands are composed of an abundance of stacking faults and twin boundaries, as indicated by the inserted SAED pattern. The HRTEM image in Fig. 3(f) further confirms the co-existence of stacking faults and twin boundaries. The microstructure of TiO_2 sample (FP at 230 mA) subjected to a compressive strain of 13.6% is also analyzed, which is same to the TiO_2 sample (FP at 280 mA) compressed to a strain of 14.7%. The parallel slip bands are composed of stacking faults and twin boundaries (see supplementary Fig. S1).

Just Accepted

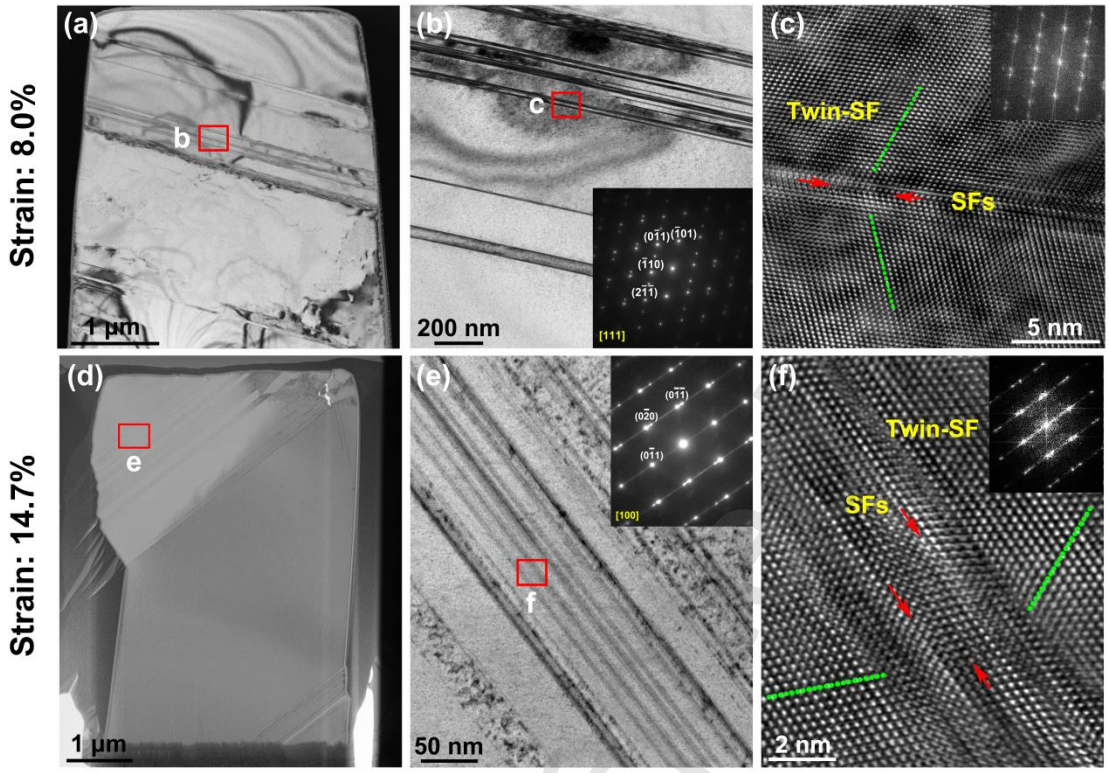


Fig. 3 TEM images of TiO_2 (FP at 280 mA) pillars after compression tests at different strains. (a,b) Low-magnification TEM image of a pillar compressed at a strain of 8.0%. (c) HRTEM image. (d,e) Low-magnification TEM image of a pillar compressed at a strain of 14.7%. (f) HRTEM image.

To investigate the microstructural changes of TiO_2 before and after FP, TEM characterization was conducted on both samples. Figure 4 presents the TEM image of the sample with FP at 280 mA. Notably, the TEM sample was prepared via conventional approach: a slice was sectioned from the central part of the cylindrical TiO_2 sample, followed by mechanical grinding and ion milling. It can be clearly seen that the sample contains a small number of stacking faults (Fig. 4(a,b)). HRTEM image shows that twin boundaries are also formed, which are decorated with stacking faults (Fig. 4(c)). However, for the pristine TiO_2 sample without FP, TEM characterization reveals clean grain interiors, virtually free of defects (see supplementary Fig. S2). These observations indicate that a small number of stacking

Just Accepted

faults and twins were generated in the sample after FP.

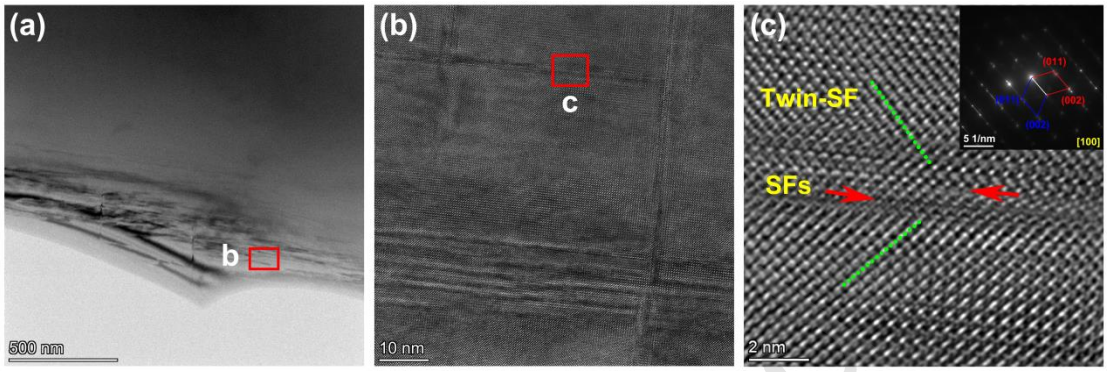


Fig. 4 TEM images of TiO_2 sample with FP at 280 mA. (a,b) TEM images showing an area of the TiO_2 containing stacking faults. (c) HRTEM image showing a twin boundary decorated with stacking faults.

The phase evolution of the TiO_2 samples before and after FP was investigated. The XRD patterns shown in Fig. 5(a) revel that all samples retain a rutile crystal structure (PDF#73-2224), indicating that no phase transformation occurs in the sample after FP. Furthermore, electron paramagnetic resonance (EPR) spectroscopy was employed to study variations in oxygen vacancies (O_V). The signal intensity of O_V (g = 2.003) is increased after FP (Fig. 5(b)), indicting an increase in oxygen vacancies after FP [32]. Notably, TiO_2 sample with FP at 280 mA contains the highest O_V concentration among them. To further quantify the relative concentration of O_V, XPS analysis was performed (Fig. 5(c-e)). The content of O_V is 57.88%, 65.31%, and 78.32% for pristine TiO_2 sample, and TiO_2 sample with FP at 230 and 280 mA, respectively (Fig. 5(f)). These results indicate that the concentration of oxygen vacancies in the TiO_2 sample is increased after FP, which also accounts for the color darkening of the sample after FP (inset of Fig. 1(b)) [33,34].

Just Accepted

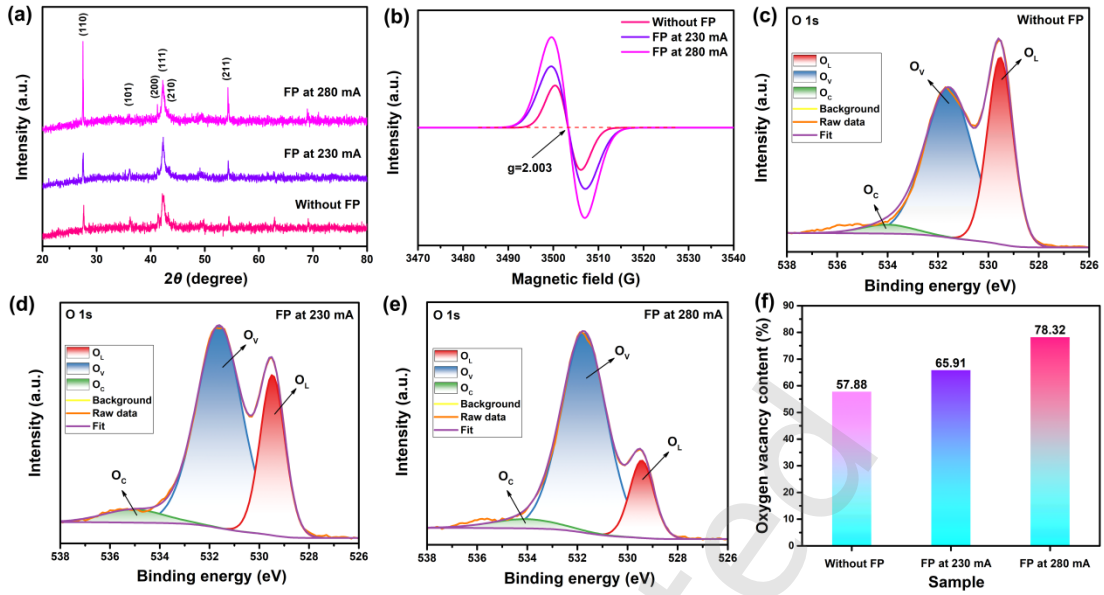


Fig. 5 (a) XRD pattern. (b) EPR spectra. (c-e) XPS spectra. (f) Content of oxygen vacancies for different samples.

4 Discussions

The micropillar compression tests at room temperature show that pristine TiO_2 samples without FP experienced brittle failure, due to strong ionic bonds, high Peierls-Nabarro lattice resistance, and insufficient active slip systems at room temperature [35,36]. Microstructural characterization of the pristine TiO_2 confirms that, apart from point defects, there is virtually no line or planar defects in the sample (see supplementary Fig. S2). These defects are normally useful for providing the active nucleation sites for dislocations to facilitate the plastic deformation [17,37]. In contrast, samples with FP exhibited substantial improvement in their plasticity at room temperature, with compressive strain reaching 15.4% without catastrophic failure (Fig. 2(e-l)). Abundant shear bands formed and multiplied during compression to accommodate the plastic deformation.

It has been reported that the plasticity could be improved even at room

Just Accepted

temperature by the introduction of high-density dislocations into ceramic materials [15-17,37]. These high-density pre-existing dislocations circumvent the dislocation nucleation, which has been identified as one of the key bottlenecks for hindering dislocation plasticity in ceramics, particularly at room temperature [16,38]. Compared to the high stress level for dislocation nucleation, these pre-existing dislocations can glide at a much low shear stress level, preventing pre-mature fracture to happen while enabling the room-temperature dislocation mobility [6,36,39]. However, in our study, we found that FP did not generate a large number of dislocations. Therefore, the room-temperature plasticity observed in our work is unlikely to be predominantly driven by dislocation-assisted plastic deformation.

4.1 Introduction of defects after FP

Detailed microstructural characterization revealed that only a small number of stacking faults and twins, along with a large quantity of oxygen vacancies, were introduced into the TiO_2 sample after FP (Fig. 4 and 5). Moreover, virtually no dislocations were observed. The stacking faults and twins may be generated during the extraordinary non-equilibrium process in FP, resulting from the coupling of electric and thermal fields [40,41]. The oxygen vacancies primarily originate from the electrochemical reduction reaction [34,42,43].

4.2 Multiplication of defects during deformation

Detailed microstructural characterization of the TiO_2 pillars deformed to a strain of 8.0% and 14.7% revealed that more stacking faults and twin boundaries were produced under successive loading in the compression tests (Fig. 3). It is indicated

Just Accepted

that multiplication of defects (stacking faults and twins) occurs during deformation. We propose that oxygen vacancies play a very important role in the multiplication of such defects. Recently, Li et al. reported that oxygen vacancies could facilitate the nucleation and propagation of stacking faults and nanotwins during compression in their study on room-temperature plasticity of flash-sintered TiO_2 [25]. Okafor et al. also reported that oxygen vacancies could facilitate the nucleation of dislocations in the $SrTiO_3$ [44]. In our study, FP introduced a large concentration of oxygen vacancies, which is expected to lower the activation energy for the nucleation and propagation of stacking faults and twins, thereby promoting their continuous generation during compression. For the TiO_2 sample with FP at 280 mA, the higher concentration of oxygen vacancies results in lower activation energy for the nucleation and propagation of defects, thereby lowering the stress required to initiate plastic deformation (Fig. 2(i-l)). With increasing strain, however, the progressive accumulation and mutual interaction of these defects increasingly impede further defect-mediated deformation, resulting in the observed work-hardening (Fig. 2(i)).

4.3 Mechanism of room-temperature plasticity

Stacking faults and twins are common planar defects in metals. It has been demonstrated that high-density stacking faults and twin boundaries enhance the strength of metal while retaining good ductility [45-48]. However, stacking faults and twins are rarely observed in most ceramics [49]. Moreover, it is extremely difficult to form the stacking faults and twins in ceramic materials [50], primarily due to the high energy penalty associated with severe distortion of strong covalent/ionic bonds.

Just Accepted

Recently, it was reported that fabrication of stacking faults and twins could significantly improve the plasticity of ceramics at room temperature [25,51-54]. Therefore, it is suggested that the room-temperature plasticity in our work is ascribed to the assistance of the stacking faults and twin boundaries. Figure 6 schematically illustrates the mechanism underlying room-temperature plastic deformation in TiO_2 with FP. Initially, a low density of stacking faults and twin boundaries, accompanied by abundant oxygen vacancies are introduced into the TiO_2 samples after FP. Upon room-temperature uniaxial compression, continuous generation and propagation of stacking faults and twin boundaries evolved into shear bands, facilitating the substantial room-temperature plastic deformability. Serrations observed on the stress-strain curves suggest the generation of stacking faults and twin boundaries during compression (Fig. 2(e-i)). The proliferation of stacking faults and twin boundaries is intimately linked to the high concentration of oxygen vacancies, which likely lowers the energy barrier for nucleation of these defects. Crucially, unlike conventional dislocation-dominated plasticity in ceramics, the room-temperature plasticity reported here operates via an oxygen-vacancy-mediated planar defect multiplication pathway.

Just Accepted

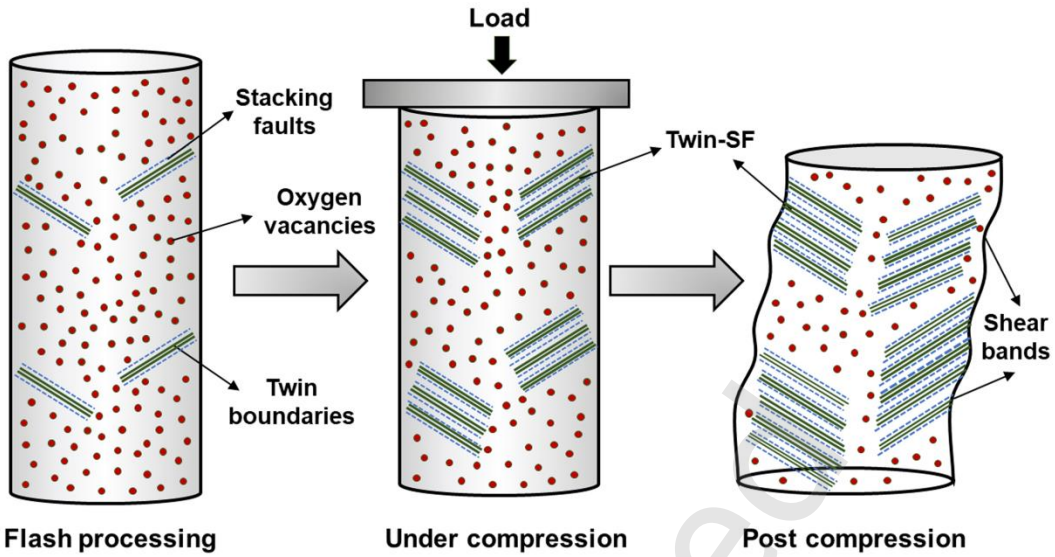


Fig. 6 Schematic illustration of the mechanism underlying room-temperature plastic deformation in TiO_2 with FP.

5 Conclusions

This study presents a universal and practical strategy for achieving the room-temperature plasticity of ceramic materials through flash pressing (FP) based on the coupling of electric and thermal fields. The micropillar compression tests revealed a large plastic compressive strain of 15.4% at room temperature could be reached for the TiO_2 ceramics after FP. Differs from the dislocation-dominated plasticity in ceramics, the room-temperature plasticity in our study is ascribed to the multiplication of stacking faults and twin boundaries during the compression, which was facilitated by the high concentration of oxygen vacancies introduced by FP. As an emerging processing technique, FP holds great potential for tailoring the microstructure and optimizing the properties of ceramic materials.

Just Accepted

Acknowledgements

This work was financially supported by the National Natural Science Foundation

of China (grant No. 52472064), the Key Research and Development Projects of Shaanxi Province (grant No. 2025CY-YBXM-144), and the Fundamental Research Funds for the Central Universities, CHD (grant No. 300102315202).

Author Contributions

Xinghua Su: Writing-review & editing, Writing-original draft, Validation, Supervision, Methodology, Funding acquisition, Formal analysis, Conceptualization. Zhenyu Li: Visualization, Validation, Methodology, Investigation, Data curation. Xufei Fang: Writing-review & editing, Methodology. Wenjun Lu: Writing-review & editing. Mengyao Wang: Investigation. Peng Zhao: Project administration.

Availability of data and materials

The data that support the findings of this study are available from the corresponding author upon reasonable request.

Competing interests

The authors have no competing interests to declare that are relevant to the content of this article.

References

[1] Ohji T, Singh M. *Engineered ceramics: Current status and future prospects*. Wiley, 2016.

Just Accepted

[2] Padture NP. Advanced structural ceramics in aerospace propulsion. *Nat Mater* 2016, **15**: 804-809.

[3] Li F, Zhang G-J, Zhou Y, et al. Expanding the members of ultra-high temperature ceramics and their maximum service temperature exceeding 3000 °C. *J Adv Ceram* 2026, **15**: 9221231.

[4] Lee WE, Gilbert M, Murphy ST, et al. Opportunities for advanced ceramics and composites in the nuclear sector. *J Am Ceram Soc* 2013, **96**: 2005-2030.

[5] Rödel J, Kounga ABN, Weissenberger-Eibl M, et al. Development of a roadmap for advanced ceramics: 2010-2025. *J Eur Ceram Soc* 2009, **29**: 1549-1560.

[6] Porz L. 60 years of dislocations in ceramics: A conceptual framework for dislocation mechanics in ceramics. *Int J Ceram Eng Sci* 2022, **4**: 214-239.

[7] Li Y, Liu X, Zhang P, et al. Theoretical insights into the Peierls plasticity in $SrTiO_3$ ceramics via dislocation remodelling. *Nat Commun* 2022, **13**: 6925.

[8] Hannink RHJ, Kelly PM, Muddle BC. Transformation toughening in zirconia-containing ceramics. *J Am Ceram Soc* 2000, **83**: 461-487.

[9] Karch J, Birringer R, Gleiter H. Ceramics ductile at low temperature. *Nature* 1987, **330**: 556-558.

[10] Becher PF. Microstructural design of toughened ceramics. *J Am Ceram Soc* 1991, **74**: 255-269.

[11] Chokshi AH. Diffusion creep in oxide ceramics. *J Eur Ceram Soc* 2002, **22**: 2469-2478.

[12] Ruano OA, Wadsworth J, Sherby OD. Deformation of fine-grained alumina by

Just Accepted

grain boundary sliding accommodated by slip. *Acta Mater* 2003, **51**: 3617-3634.

[13] Korte S, Clegg WJ. Micropillar compression of ceramics at elevated temperatures. *Scripta Mater* 2009, **60**: 807-810.

[14] Liu C, Shen C, Shen J. In situ studies on microstructural evolution and thermally activated plasticity of (Co,Cu,Mg,Ni,Zn)O high-entropy oxide. *Acta Mater* 2026, **312**: 122212.

[15] Dong LR, Zhang J, Li YZ, et al. Borrowed dislocations for ductility in ceramics. *Science* 2024, **385**: 422-427.

[16] Fang X, Lu W, Zhang J, et al. Harvesting room-temperature plasticity in ceramics by mechanically seeded dislocations. *Mater Today* 2025, **82**: 81-91.

[17] Shen C, Li J, Niu T, et al. Achieving room temperature plasticity in brittle ceramics through elevated temperature preloading. *Sci Adv* 2024, **10**: eadj4079.

[18] Cologna M, Rashkova B, Raj R. Flash sintering of nanograin zirconia in <5 s at 850 °C. *J Am Ceram Soc* 2010, **93**: 3556-3559.

[19] Biesuz M, Sglavo VM. Flash sintering of ceramics. *J Eur Ceram Soc* 2019, **39**: 115-143.

[20] Yoon B, Avila V, Lavagnini IR, et al. Reactive flash sintering of ceramics: A review. *Adv Eng Mater* 2023, **25**: 2200731.

[21] Liu D, Shao G, Tai X, et al. Field-assisted sintering: Overview of thermo-electro-mechanical coupling effects. *J Adv Ceram* 2026, **15**: 9221276.

[22] Liu Z, He Z, Li Z, et al. Large-diameter ceramic room-temperature flash sintering technology based on new carbon electrodes. *J Adv Ceram* 2025, **14**: 9221094.

Just Accepted

[23] Su X, Zeng H, Tian Y, et al. Influence of pre-sintering on the reactive flash sintering of high-entropy rare earth zirconate ceramics. *J Eur Ceram Soc* 2026, **46**: 117901.

[24] Cho J, Li Q, Wang H, et al. High temperature deformability of ductile flash-sintered ceramics via in-situ compression. *Nat Commun* 2018, **9**: 2063.

[25] Li J, Cho J, Ding J, et al. Nanoscale stacking fault-assisted room temperature plasticity in flash-sintered TiO_2. *Sci Adv* 2019, **5**: eaaw5519.

[26] Chen K, Yuan X, Tian Z, et al. A facile approach for generating ordered oxygen vacancies in metal oxides. *Nat Mater* 2025, **24**: 835-842.

[27] Guillon O, De Souza RA, Mishra TP, et al. Electric-field-assisted processing of ceramics: Nonthermal effects and related mechanisms. *MRS Bull* 2021, **46**: 52-58.

[28] Rheinheimer W, Phuah XL, Wang H, et al. The role of point defects and defect gradients in flash sintering of perovskite oxides. *Acta Mater* 2019, **165**: 398-408.

[29] Biesuz M, Karacasulu L. Ultra-fast sintering and grain boundary metastability in ceramics. *Curr Opin Solid State Mater Sci* 2026, **42**: 101258.

[30] Takeuchi S, Hashimoto T. Deformation mechanisms in titanium dioxide single crystals. *J Mater Sci* 1990, **25**: 417-423.

[31] Raj R. Joule heating during flash-sintering. *J Eur Ceram Soc* 2012, **32**: 2293-2301.

[32] Zhang X, Wang L, Wei J, et al. Dynamic oxygen vacancy engineering on CuO via refreshable catalytic surface for high-efficient water decontamination. *Nat Commun* 2026, **17**: 1432.

Just Accepted

[33] Yang Y, Yin L-C, Gong Y, et al. An unusual strong visible-light absorption band in red anatase TiO_2 photocatalyst induced by atomic hydrogen-occupied oxygen vacancies. *Adv Mater* 2018, **30**: 1704479.

[34] Su X, Li W, Chen D, et al. Rapid fabrication of oxygen-deficient zirconia by flash sintering treatment. *J Adv Ceram* 2024, **13**: 1881-1890.

[35] Bajla A, Majumder S, Mubassira S, et al. Toughening of TiO_2 via femtosecond laser shock peening. *J Am Ceram Soc* 2026, **109**: e71037.

[36] Fang X. A dislocation perspective on strength and toughness in ceramics. *Adv Eng Mater* 2026, **28**: e70965.

[37] Frisch A, Okafor C, Preuß O, et al. Room-temperature dislocation plasticity in ceramics: Methods, materials, and mechanisms. *J Am Ceram Soc* 2025, **108**: e20575.

[38] Fang X. Mechanical tailoring of dislocations in ceramics at room temperature: A perspective. *J Am Ceram Soc* 2024, **107**: 1425-1447.

[39] Fang X, Zhang J, Frisch A, et al. Room-temperature bulk plasticity and tunable dislocation densities in $KTaO_3$. *J Am Ceram Soc* 2024, **107**: 7054-7061.

[40] Xue S, Li Phuah X, Jian J, et al. In situ studies on defect formation dynamics in flash-sintered TiO_2. *Nanoscale* 2023, **15**: 16752-16765.

[41] Yang B, Shang Z, Li J, et al. Effects of electric field on microstructure evolution and defect formation in flash-sintered TiO_2. *J Eur Ceram Soc* 2022, **42**: 6040-6047.

[42] Eqbal A, Chakrabarti T. Study on the electrochemical effect of ZnO addition on flash sintering of 3 mol% yttria stabilized zirconia. *J Eur Ceram Soc* 2023, **43**: 6260-6271.

Just Accepted

[43] Biesuz M, Pinter L, Saunders T, et al. Investigation of electrochemical, optical and thermal effects during flash sintering of 8YSZ. *Materials* 2018, **11**: 1214.

[44] Okafor C, Sayyadi-Shahraki A, Bruns S, et al. Coupled electromigration-nanoindentation study on dislocation nucleation in $SrTiO_3$. *J Am Ceram Soc* 2025, **108**: e70015.

[45] Lu L, Shen Y, Chen X, et al. Ultrahigh strength and high electrical conductivity in copper. *Science* 2004, **304**: 422-426.

[46] Zhang YF, Xue S, Li Q, et al. Size dependent strengthening in high strength nanotwinned Al/Ti multilayers. *Acta Mater* 2019, **175**: 466-476.

[47] Wu X, Zhu YT, Chen MW, et al. Twinning and stacking fault formation during tensile deformation of nanocrystalline Ni. *Scr Mater* 2006, **54**: 1685-1690.

[48] Feng X, Zhang J, Wu K, et al. Ultrastrong $Al_{0.1}$CoCrFeNi high-entropy alloys at small scales: effects of stacking faults vs. nanotwins. *Nanoscale* 2018, **10**: 13329-13334.

[49] Su R, Neffati D, Zhang Y, et al. The influence of stacking faults on mechanical behavior of advanced materials. *Mater Sci Eng A* 2021, **803**: 140696.

[50] Chen Y, Guo T, Pang X, et al. Formation of high-density stacking faults in ceramic films induced by Ti transition layer. *Scripta Mater* 2022, **211**: 114496.

[51] Liu L, An X, Gu X, et al. Nanotwinned CrN ceramics with enhanced plasticity. *Nat Commun* 2025, **16**: 5934.

[52] Huang Y, Chen Z, Meindlhumer M, et al. Harvesting superior intrinsic plasticity in nitride ceramics with negative stacking fault energy. *Acta Mater* 2025, **286**:

Just Accepted

120774.

[53] Yu J, Ding R, Liu Y. Stacking fault energy engineering as the pathway to materials with exceptional performance. *Adv Mater* 2026, https://doi.org/10.1002/adma.73385.

[54] Xu Z, Zhang J, Dong L, et al. Rethinking brittleness in ceramics: The emergence of room-temperature plasticity. *J Adv Ceram* 2026, **15**: 9221353.

Just Accepted